

Universal mechanism for electron paramagnetic resonance of individual adatoms

J. L. Lado,¹ A. Ferrón,² and J. Fernández-Rossier^{1,3}

¹ *QuantaLab, International Iberian Nanotechnology Laboratory (INL),
Av. Mestre José Veiga, 4715-330 Braga, Portugal*

² *Instituto de Modelado e Innovación Tecnológica (CONICET-UNNE) and Facultad de Ciencias Exactas,
Naturales y Agrimensura, Universidad Nacional del Nordeste,
Avenida Libertad 5400, W3404AAS Corrientes, Argentina.*

³ *Departamento de Física Aplicada, Universidad de Alicante, 03690 Spain*
(Dated: November 4, 2016)

We propose a new universal mechanism that makes it possible to drive an individual atomic spin using a spin polarized scanning tunnel microscope (STM) with an oscillating electric signal. We show that the combination of the distance dependent exchange with the magnetic tip and the electrically driven mechanical oscillation of the surface spins permits to control their quantum state. Based on a combination of density functional theory and multiplet calculations, we show that the proposed mechanism is essential to account for the recently observed electrically driven paramagnetic spin resonance (ESR) of an individual Fe atom on a MgO/Ag(100) surface. Our findings set the foundation to deploy the ESR-STM quantum sensing technique to a much broader class of systems.

Scanning tunneling microscopy (STM) and electron paramagnetic resonance (EPR) are two very powerful experimental techniques whose integration has been pursued in the last 3 decades[1–6] and motivated a substantial body of theoretical work[7–9]. In EPR, spin transitions are excited with an ac field that permits to resolve spin excitation with a resolution limited by the intrinsic spin relaxation broadening of the species. In continuous wave (cw) EPR this can be down to a few MHz for amorphous hydrogenated silicon [10]. However, standard detection techniques based on induction require probing at least 10^7 spins[11], and have thereby a very poor spatial resolution. In contrast, STM permits to probe individual atoms with an exquisite spatial resolution, but when it comes to perform spin spectroscopy, it relies on inelastic electron tunneling[12] (IETS), whose spectral resolution is limited[13] by $5.4k_B T$, where T is the temperature. Thus, even for the coldest STM so far[14], the spectral resolution of IETS spectroscopy would be above 30 GHz, ie, 3 orders of magnitude worse off than cw-EPR.

In a recent experimental breakthrough, Baumann *et al.* [6] have reported the measurement of the electron paramagnetic resonance of an individual Fe atom deposited on top of an atomically thin MgO layer grown on Ag(001), using an spin polarized STM tip (see figure 1) to both drive the atom with an ac signal and to probe the resulting reaction. For the driving, they applied a radio frequency (RF) voltage V_{RF} across the tip-sample with frequency f . The resulting change in dc current, I_{DC} as a function of f displayed a very narrow (3MHz) resonance peak, at the frequency f_0 that matches the Zeeman splitting of the magnetic adatom ground state doublet. The peak, well above the noise level, would shift upon application of a magnetic field, making it possible thereby to detect $50\mu T$ variations with subatomic resolution.

The experiment of Baumann *et al.* [6], electrically driven paramagnetic spin resonance (ESR), outperforms

the spectral resolution of IETS-STM spectroscopy by 4 orders of magnitude, at the same temperature, and reaches the absolute detection limit, by probing a single spin. The recently reported application of this remarkable setup to probe the magnetic moment of individual atoms nearby [15, 16] demonstrates the potential of ESR-STM technique as an extremely versatile quantum sensing tool.

In this paper we address a fundamental question that begs for an answer in order to understand the working principles of any STM-ESR setup, namely, how an RF voltage can drive the atomic spin. Baumann *et al.* [6] proposed a mechanism that combines two ingredients. First, the RF electric field induces a mechanical oscillation $z(t)$ of the surface atom. Second, the induced modulation of the crystal field, combined with the spin-orbit interaction of the d electrons of the surface atom, results in transitions between the two lowest energy levels of the atomic spin. Whereas the first ingredient applies for any charged surface atom, the second is only valid for the specific symmetry of the Fe/MgO system.

Here we propose an alternative universal mechanism that permits to drive the spin of a charged surface atom, using an RF electrical voltage and an STM tip with a magnetic atom in the apex. The mechanism is based on the notion that spin interactions between the tip and the surface atom depend strongly on their distance. The electric modulation of the surface atom position results in a variation of the spin-spin interaction that can efficiently drive the surface spin.

When a voltage difference $V_{RF}(t)$ is applied across the gap between the tip and the sample the electric field induces a small vertical displacement of the surface atom $z(t)$ (see Fig. 1b). We can Taylor expand the spin Hamiltonian of the surface atom around $z = 0$, the surface atom

equilibrium position:

$$\mathcal{H} \approx \mathcal{H}_0 + z(t) \frac{\partial \mathcal{H}}{\partial z} \Big|_{z=0} \quad (1)$$

Transitions between a given pair of eigenstates of the atomic spin Hamiltonian \mathcal{H}_0 , $|M\rangle$ and $|N\rangle$, will be induced provided that the Rabi force $\mathcal{F}_{\mathcal{N},\mathcal{M}} = \langle N | \frac{\partial \mathcal{H}}{\partial z} | M \rangle \neq 0$. Several terms in the Hamiltonian can yield a non-zero contribution to the term $\frac{\partial \mathcal{H}}{\partial z}$, whose physical meaning is related on how the Hamiltonian felt by the surface spin changes under small displacements of the surface atom, and is the responsible of coupling the surface spin to an electrical signal. In this letter we propose that the variation on the tip-surface distance provides such coupling in the form of direct exchange interaction $\mathcal{H}_J = J(z(t)) \vec{S}_T \cdot \vec{S}$. Such contribution, already studied theoretically and observed experimentally [17–21], will be present in any surface spin when probed with a spin polarized STM and therefore represents a universal mechanism for electron paramagnetic resonance of individual adatoms.

We ignore the quantum fluctuations of the magnetic moment of the apex atom, quenched by the combination of an applied magnetic field and strong Korringa damping with the tip electron bath. Therefore, we treat the tip spin in a mean field or classical approximation, following Yan et al.[20], and replace \vec{S}_T by its statistical average $\langle \vec{S}_T \rangle$. For the sake of simplicity, we will restrict the discussion to the case when the dynamics is restricted to the two lowest energy states $|0\rangle$ and $|1\rangle$, although our description of the atomic spin states includes hundreds of multi-electron configurations, as we describe below [22, 23]. Within the two-level approximation, the relevant operator for the Rabi force associated with the exchange interaction is

$$\mathcal{F}_J = \frac{\partial J(z)}{\partial z} \langle \vec{S}_T \rangle \cdot \langle 0 | \vec{S} | 1 \rangle \quad (2)$$

This mechanism does not rely on the specifics of the crystal field of the adatom nor on spin-orbit coupling, suggesting the possibility to apply the single spin STM-ESR to a variety of systems, including S=1/2 atoms and light element magnetism.[24]

A different mechanism was proposed by Baumann *et al.* [6] specific for Fe on the (100) MgO surface, where the combination of crystal field and spin-orbit interaction would couple the two lowest energy levels of the atomic spin. The relevant Rabi force for this crystal field mechanism reads

$$\mathcal{F}_{CF} = \frac{\partial F_W}{\partial z} \langle 0 | l_x^4 + l_y^4 | 1 \rangle \quad (3)$$

where F_W is a crystal field parameter, l_x and l_y are the single-particle orbital momentum operator for the d electrons of the surface Fe.

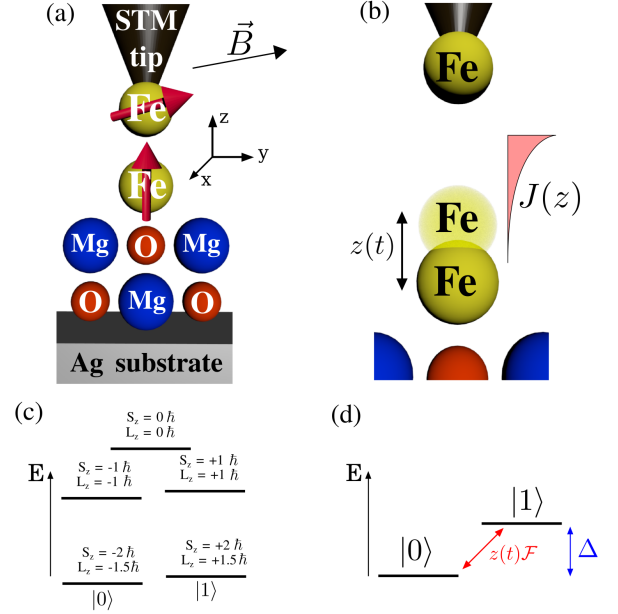


FIG. 1: (a) Sketch of an Fe atom in MgO, where the ESR signal will be measured with an STM tip. The electric field created by the tip moves the Fe atom upwards and downwards as shown in (b), in particular changing the the exchange interaction $J(z)$. Panel (c) shows a sketch of the energy levels of Fe on MgO in the presence of a small off-plane magnetic field ($B_z = 0.2$ T). Panel (d) shows the reduced low energy Hamiltonian, restricting the dynamics to the two lowest energy levels in (c).

A third mechanism is provided by the dipolar interaction between the magnetic moment of the tip and the Fe atom on the surface, where the tip creates an z -dependent in-plane magnetic field, giving rise a dipolar mixing term of the form

$$\mathcal{F}_{\text{dip}} = \mu_B \frac{\partial B_x^{\text{Tip}}}{\partial z} \langle 0 | L_x + 2S_x | 1 \rangle \quad (4)$$

where $B_x^{\text{Tip}} = 2 \frac{\mu_0}{4\pi} \frac{\mu_B S_x^{\text{Tip}}}{d_{\text{Fe-Tip}}^3}$ is the magnetic field created by the tip, assuming the moment of the tip lies in-plane and $d_{\text{Fe-Tip}}^3$ is the tip-Fe distance.

For the three mechanisms, the resulting two-level system can be written as $\mathcal{H}_{\text{eff}} = \frac{\Delta}{2} \tau_z + \hbar \Omega(t) \tau_x$, with τ_z, τ_x the Pauli matrices in the $|0\rangle, |1\rangle$ subspace, $\Delta = \hbar \omega_0$ the splitting between the ground state and the first excited, with the driving Rabi term

$$\Omega(t) = \frac{\mathcal{F}}{\hbar} z(t) \quad (5)$$

Due to the oscillating electrical signal applied, $z(t) = z_0 \cos \omega t$, with $z_0 \propto V_{\text{RF}}(t)$, we can write down $\Omega(t) = \Omega_0 \cos \omega t$. We refer to $\Omega_0 = \mathcal{F} z_0 / \hbar$ as the Rabi frequency, which quantifies the efficiency of the driving mechanism and determines the Rabi time $\tau = \pi / \Omega_0$. This driving force competes with the spin relaxation,

characterized by the longitudinal and transverse spin relaxation times, T_1 and T_2 , as described by the Bloch equations[25]. Within this approximation, the steady state solution for the population difference between the ground and excited states is given by the resonance curve $P_0 - P_1 = \coth\left(\frac{\hbar\omega_0}{2k_B T}\right) \left(1 - \frac{\Omega_0^2 T_1 T_2}{1 + (\omega - \omega_0)^2 T_2^2 + \Omega_0^2 T_1 T_2}\right)$ where P_1 and P_0 are the occupation of the ground and excited state, respectively, k_B Boltzmann's constant, T the temperature and the first term on the right-hand side is the thermal equilibrium solution. Together with T_1 and T_2 , Ω_0 is critical to assess by how much $P_1 - P_0$ departs from its equilibrium value.

We now elaborate on the microscopic nature of the operator $\hat{\mathcal{F}} = \frac{\partial \mathcal{H}}{\partial z}$ relevant for the three mechanisms under discussion. For the crystal field mechanism[6], the vertical displacement of the Fe adatom, $z(t)$ modifies the crystal field created by the 4 closest Mg ions on the surface (see Fig. 1b), which in turn modulate the quartic term that allows direct mixing between $L_z = \pm 2$ [26]. The interatomic exchange, that arises from the overlap of the tails of the atomic orbitals, decays exponentially but can be very large at short distances. In the following we parametrize $J(z) = J_0 e^{-z/\ell}$, with $\ell = 0.06$ nm [20] and $J_0 = 2$ meV [19, 20], assuming the tip-Fe distance is $d_{\text{Fe-Tip}} = 0.6$ nm and $\langle \vec{S}_T \rangle = 2\hbar$.

The RF bias can induce a Rabi oscillation by means of the three different mechanisms, crystal field (Eq. 3), exchange (Eq. 2) and dipolar (Eq. 4). The Rabi frequency for all mechanisms depends on the amplitude of the oscillation (Eq. 5), that is modulated by the AC bias. Therefore, the mechanism responsible of the oscillation can be determined by comparing the relative sizes of the Rabi forces \mathcal{F}_J , \mathcal{F}_{CF} and \mathcal{F}_{dip} . For the exchange mechanism, the exponential dependence of the exchange coupling implies that the prefactor in Eq. 2 takes a value $\frac{\partial J(z)}{\partial z} \langle \vec{S}_T \rangle = 66.7$ meV/nm. The prefactor for the dipolar mechanism as given by Eq. 4 yields $\mu_B \frac{\partial B_x^{\text{Tip}}}{\partial z} = 0.02$ meV/nm, much smaller than the exchange mechanism and therefore negligible for typical Tip-Fe distances for ESR. Finally, the prefactor for the crystal field mechanism in Eq. 3 requires knowledge of the local crystal field of Fe.

For that matter, we need a spin Hamiltonian for Fe on MgO and, importantly, how it depends on z_0 . We derive it starting from a density functional theory (DFT) calculation[27] for the system, following the same procedure described in previous works[22, 23]. We build a few level model for the electrons in the d orbitals of Fe, including the crystal field, spin-orbit coupling and electron-electron interaction and we solve it by numerical diagonalization. The crystal field part of the Hamiltonian is obtained from the representation of the DFT Hamiltonian in the basis of maximally localized Wannier orbitals[28, 29] $\mathcal{H}_{\text{CF}}(z) = D_W(z)l_z^2 + F_W(z)(l_x^4 + l_y^4)$ where $D_W(z)$ and $F_W(z)$ are crystal field parameters that de-

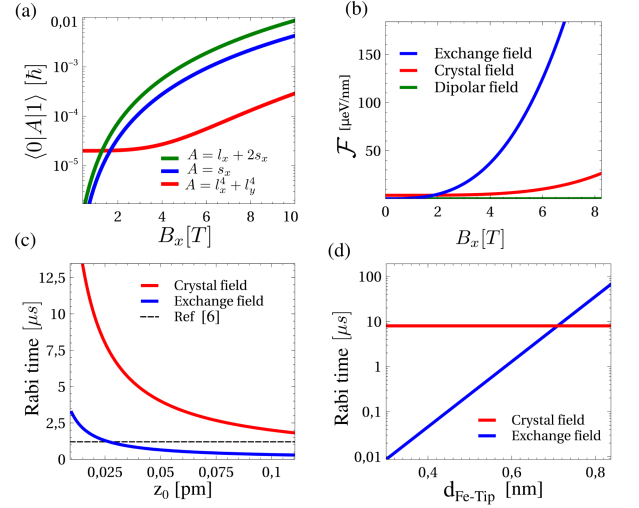


FIG. 2: (a) Matrix elements between the ground and first excited state for the square field perturbation, in-plane Zeeman perturbation and in-plane exchange perturbation. With the previous matrix elements and the dependence of the Hamiltonian with z , the Rabi force can be calculated (b), yielding that the strongest contribution is the exchange mechanism. The Rabi time can be calculated from the Rabi frequency Eq. 5 provided the displacement z_0 is known, shown in (c). The exponential dependence of the exchange field produces that the exchange Rabi time depends on the Fe-Tip distance, while the crystal field mechanism is assumed independent (d).

pend on the vertical coordinate of the surface Fe atom z . On top of that we add the spin-orbit coupling operator $\mathcal{H}_{\text{SOC}} = \lambda_{\text{SOC}} \vec{l} \cdot \vec{s}$ with $\lambda_{\text{SOC}} = 35$ meV, the Zeeman term $\mathcal{H}_B = \mu_B \vec{B} \cdot (\vec{l} + 2\vec{s})$ and the electron-electron Coulomb interaction in the d shell.

Importantly, the Wannierization procedure permits to compute both the coefficients D_W and F_W and how they change with the vertical Fe displacement z . For equilibrium $z = 0$ we find $F_W = -10$ meV [32], $D_W = -290$ meV[33], $\frac{\partial F_W}{\partial z}|_{z=0} = 280$ meV/nm and $\lambda_{\text{SOC}} = 35$ meV. In particular, we also find that the two lowest energy states $|0\rangle$ and $|1\rangle$ of the Hamiltonian eigenstates of $\mathcal{H}_0 \equiv \mathcal{H}(z)$ have a strong overlap with the states with quantum numbers $|L = 2, S = 2, L_z = \pm 2, S_z = \pm 2\rangle$. This is why the energy difference Δ is very sensitive to the application of an off-plane field B_z , and quite insensitive to in-plane components, B_x, B_y .

The results obtained with our method confirm the phenomenological Hamiltonian describing the low energy multi-electronic states for 6 electrons in the d levels of Fe, in the crystal field of the MgO(100) surface, proposed by Baumann *et al.* [6, 30]. In particular, the low energy sector of the Hamiltonian can be parametrized with $\mathcal{H}(z) = DL_z^2 + F(L_+^4 + L_-^4) + \Lambda \vec{L} \cdot \vec{S} + \mu_B \vec{B} \cdot (\vec{L} + 2\vec{S})$ where L_a are the many-body angular momentum operators in the subspace $L = 2$, \vec{S} are spin operators in the

$S = 2$ subspace, in both cases complying with atomic Hund's rules. By fitting the energies and orbital expectation values of the lowest 5 states between the multiplet and spin Hamiltonians, we find the relations $D = -160$ meV, $F = -2$ meV and $\Lambda = -11$ meV, that permit to connect the DFT calculation with the spin model in a simple manner.

The derivation of the atomic spin Hamiltonian from DFT permits to compute the relevant matrix elements for the three mechanisms (Fig. 2a), as well as the Rabi forces (Fig. 2b). The matrix elements in Fig. 2a show that the biggest off-diagonal terms correspond to the spin operator s_x rather than the crystal field operator $l_x^4 + l_y^4$ at finite in-plane magnetic fields, giving an advantage to the exchange over the crystal field mechanism. When the full Rabi force is calculated, Fig. 2b, it is obtained that the exchange remains the leading mechanism, followed by the crystal field, whereas the dipolar contribution is nearly negligible. The role of the in-plane magnetic field (applied along the x-axis) is to mix the wave functions of $|0\rangle$ and $|1\rangle$ with eigenstates with different S_z , which finally enables the transitions between them.

The actual value of the Rabi frequency depends on the magnitude of the displacement z_0 . First, we take the value of z_0 as a free parameter and show how the Rabi time depends on it. In Fig. 2c we show the Rabi time as a function of the Fe displacement z for the crystal field and exchange mechanisms, as well as the experimental value as a dashed line. The value of the Fe displacement that would yield a Rabi time comparable to the experiment would be around $z = 0.025$ pm. In the following we estimate the magnitude of the vertical displacement assuming equilibrium between the electric force $F_{\text{el}} = q_{\text{atom}} E_{\text{RF}}(t)$ and the spring constant $F_{\text{res}} = -kz$, where k is the restoring force. As the driving frequency is in the GHz range, much smaller than the standard frequency of stretching modes, $\omega_{\text{Fe}} = \sqrt{\frac{k}{M_{\text{Fe}}}}$, in the THz, we can assume that the atom is always at the instantaneous equilibrium position

$$z(t) = \frac{q_{\text{atom}}}{k} \frac{V_{\text{RF}}(t)}{d} \quad (6)$$

with d the decay distance of the electric field, on the order of the Fe-Tip distance. DFT calculations yield a value of $k \approx 600$ eV/nm², that for $q = 2e$ (Fe²⁺), $d = d_{\text{Tip-Fe}} = 0.6$ nm and $V = 8$ meV [6] gives a value for the Fe displacement of $z = 0.044$ pm, comparable with the one needed for the Rabi time associated with the exchange field. For reference, the iron oxide Young modulus [31] would give $z = 0.11$ pm. We note that the previous estimate would show sizable variations if noninteger charging of Fe ($q \leq 2$) or finite voltage drop length ($d > 0.6$ nm) are considered.

The two leading mechanisms, exchange and crystal field, show a crossover depending on the tip-Fe distance.

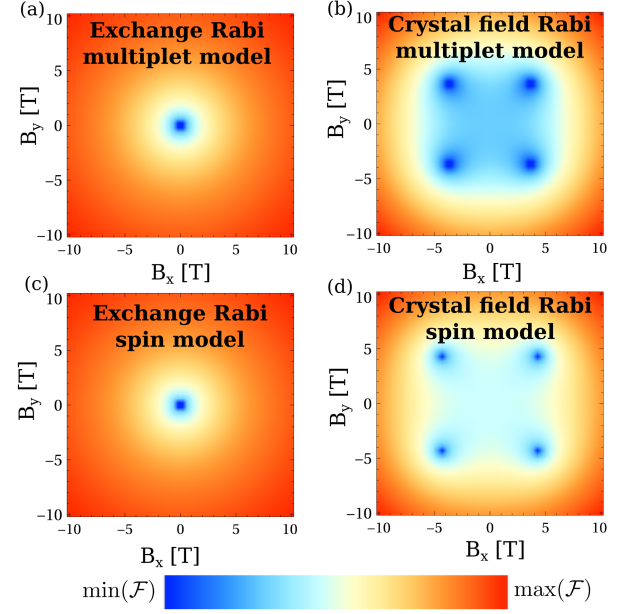


FIG. 3: Rabi forces for the exchange (a,c) and crystal field (b,d) ESR mechanisms, as a function of the two components of the in-plane field. Panels (a,b) correspond to the multiplet model and panels (c,d) to the spin model. The crystal field contribution shows nodes when the magnetic field is applied in the (11) directions, whereas the exchange mechanism is isotropic. Such symmetry difference allows to determine the leading mechanism experimentally.

Assuming the Fe displacement z_0 constant, the exchange Rabi force decreases exponentially with Fe-tip distance for the exchange mechanism, while the crystal field will be more or less constant. This leads to a dominance of exchange at intermediate distances, and a dominance of the crystal field mechanism at large distances, as shown in Fig. 2d.

We now propose an experimental test to infer which of the proposed mechanisms is actually driving the spins in the case of Fe on MgO, based on the dependence of the Rabi energy on the orientation of the in-plane magnetic field. For that matter, we plot the Rabi forces, both for the exchange and crystal field mechanisms, as a function of B_x and B_y (Fig. 3). For reference, the states are computed both with the spin model and with the full multiplet calculation. For the exchange mechanism we obtain a quite isotropic behavior, expected from the scalar nature of this interaction. In contrast, for the crystal field mechanism, the map reflects the C_4 local symmetry, developing nodes in the (11) direction (Fig. 3b,d). This same analysis could be carried out to distinguish the relevant mechanism for other atoms deposited on different surfaces. In case the dominant mechanism is crystal field, this makes possible to determine the local distortions by observing the symmetry of the Rabi response with the in-plane magnetic fields.

In conclusion, we have shown that a modulated exchange coupling between a surface atom and a magnetic STM tip is an efficient mechanism to induce electron paramagnetic resonance in the surface spin, by inducing a Rabi oscillation between the two lowest states. Our calculations based on DFT and multiplet calculations show that this mechanism accounts for the Rabi time measured in the experiment, in comparison with the too large one predicted by the crystal field mechanism. Importantly, the exchange driven mechanism shows that the ESR technique is way more general and could be realized in systems that do not have a specific crystal field and a sizable spin-orbit coupling.

Acknowledgments We acknowledge financial support by Marie-Curie-ITN 607904 SPINOGRAPH. JFR acknowledges financial supported by MEC-Spain (FIS2013-47328-C2-2-P) and Generalitat Valenciana (ACOMP/2010/070), Prometeo. AF acknowledges CONICET (PIP11220150100327) and FONCyT (PICT-2012-2866). We thank A. Heinrich and F. Delgado for useful discussions.

-
- [1] Y Manassen, RJ Hamers, JE Demuth, and AJ Castellano Jr. Direct observation of the precession of individual paramagnetic spins on oxidized silicon surfaces. *Physical review letters*, 62(21):2531, 1989.
 - [2] C Durkan and ME Welland. Electronic spin detection in molecules using scanning-tunneling-microscopy-assisted electron-spin resonance. *Applied physics letters*, 80(3):458–460, 2002.
 - [3] Tadahiro Komeda and Yishay Manassen. Distribution of frequencies of a single precessing spin detected by scanning tunneling microscope. *Applied Physics Letters*, 92(21):212506, 2008.
 - [4] Alexander V Balatsky, Mitsuaki Nishijima, and Yishay Manassen. Electron spin resonance-scanning tunneling microscopy. *Advances in Physics*, 61(2):117–152, 2012.
 - [5] Stefan Müllegger, Stefano Tebi, Amal K. Das, Wolfgang Schöfberger, Felix Faschinger, and Reinhold Koch. Radio frequency scanning tunneling spectroscopy for single-molecule spin resonance. *Phys. Rev. Lett.*, 113:133001, Sep 2014.
 - [6] Susanne Baumann, William Paul, Taeyoung Choi, Christopher P Lutz, Arzhang Ardavan, and Andreas J Heinrich. Electron paramagnetic resonance of individual atoms on a surface. *Science*, 350(6259):417–420, 2015.
 - [7] AV Balatsky, Yishay Manassen, and Ran Salem. ESR-stm of a single precessing spin: Detection of exchange-based spin noise. *Physical Review B*, 66(19):195416, 2002.
 - [8] L. N. Bulaevskii, M. Hruška, and G. Ortiz. Tunneling measurement of quantum spin oscillations. *Phys. Rev. B*, 68:125415, Sep 2003.
 - [9] Alvaro Caso, Baruch Horovitz, and Liliana Arrachea. Model for electron spin resonance in stm noise. *Phys. Rev. B*, 89:075412, Feb 2014.
 - [10] Deborah G Mitchell, Mark Tseitlin, Richard W Quine, Virginia Meyer, Mark E Newton, Alexander Schnegg, Benjamin George, Sandra S Eaton, and Gareth R Eaton. X-band rapid-scan epr of samples with long electron spin relaxation times: a comparison of continuous wave, pulse and rapid-scan epr. *Molecular Physics*, 111(18-19):2664–2673, 2013.
 - [11] Aharon Blank, Curt R Dunnam, Peter P Borbat, and Jack H Freed. High resolution electron spin resonance microscopy. *Journal of Magnetic Resonance*, 165(1):116–127, 2003.
 - [12] C. Hirjibehedin, C-Y Lin, A.F. Otte, M. Ternes, C. P. Lutz, B. A. Jones, and A. J. Heinrich. Large magnetic anisotropy of a single atomic spin embedded in a surface molecular network. *Science*, 317:1199, 2007.
 - [13] R. C. Jaklevic and J. Lambe. Molecular vibration spectra by electron tunneling. *Phys. Rev. Lett.*, 17:1139, 1966.
 - [14] Maximilian Assig, Markus Etzkorn, Axel Enders, Wolfgang Stiepany, Christian R Ast, and Klaus Kern. A 10 mk scanning tunneling microscope operating in ultra high vacuum and high magnetic fields. *Review of Scientific Instruments*, 84(3):033903, 2013.
 - [15] T Choi, W Paul, S Rolf-Pissarczyk, A Macdonald, K Yang, FD Natterer, CP Lutz, and AJ Heinrich. Magnetic dipole-dipole sensing at atomic scale using electron spin resonance stm. *Bulletin of the American Physical Society*, 2016.
 - [16] Fabian D Natterer, Kai Yang, William Paul, Philip Willke, Taeyoung Choi, Thomas Greber, Andreas J Heinrich, and Christopher P Lutz. Reading and writing single-atom magnets. *arXiv:1607.03977*, 2016.
 - [17] R. Schmidt, C. Lazo, H. Hölscher, U. H. Pi, V. Caciuc, A. Schwarz, R. Wiesendanger, and S. Heinze. Probing the magnetic exchange forces of iron on the atomic scale. *Nano Lett.*, 9:200–204, 2009.
 - [18] Kun Tao, V. S. Stepanyuk, W. Hergert, I. Rungger, S. Sanvito, and P. Bruno. Switching a single spin on metal surfaces by a stm tip: Ab initio studies. *Phys. Rev. Lett.*, 103:057202, 2009.
 - [19] R. Schmidt, C. Lazo, U. Kaiser, A. Schwarz, S. Heinze, and R. Wiesendanger. Quantitative measurement of the magnetic exchange interaction across a vacuum gap. *Phys. Rev. Lett.*, 106:257202, Jun 2011.
 - [20] Shichao Yan, Deung-Jang Choi, Jacob AJ Burgess, Stefan Rolf-Pissarczyk, and Sebastian Loth. Control of quantum magnets by atomic exchange bias. *Nature nanotechnology*, 10(1):40–45, 2015.
 - [21] Matthias Muenks, Peter Jacobson, Markus Ternes, and Klaus Kern. Correlation driven transport asymmetries through coupled spins. *arXiv preprint arXiv:1605.02798*, 2016.
 - [22] Alejandro Ferrón, Fernando Delgado, and Joaquín Fernández-Rossier. Derivation of the spin hamiltonians for fe in mgo. *New Journal of Physics*, 17(3):033020, 2015.
 - [23] A. Ferrón, J. L. Lado, and J. Fernández-Rossier. Electronic properties of transition metal atoms on cu₂N/Cu(100). *Phys. Rev. B*, 92:174407, Nov 2015.
 - [24] Héctor González-Herrero, José M Gómez-Rodríguez, Pierre Mallet, Mohamed Moaied, Juan José Palacios, Carlos Salgado, Miguel M Ugeda, Jean-Yves Veuillen, Félix Yndurain, and Iván Brihuega. Atomic-scale control of graphene magnetism by using hydrogen atoms. *Science*, 352(6284):437–441, 2016.
 - [25] A. Abragam and B. Bleaney. *Electron Paramagnetic Resonance of Transition Ions*. Oxford University Press, Oxford, 1970.

- ford, 1970.
- [26] S. Baumann, F. Donati, S. Stepanow, S. Rusponi, W. Paul, S. Gangopadhyay, I. G. Rau, G. E. Pacchioni, L. Gragnaniello, M. Pivetta, J. Dreiser, C. Piamonteze, C. P. Lutz, R. M. Macfarlane, B. A. Jones, P. Gambardella, A. J. Heinrich, and H. Brune. Origin of perpendicular magnetic anisotropy and large orbital moment in fe atoms on mgo. *Phys. Rev. Lett.*, 115:237202, Dec 2015.
 - [27] Paolo Giannozzi, Stefano Baroni, Nicola Bonini, Matteo Calandra, Roberto Car, Carlo Cavazzoni, Davide Ceresoli, Guido L Chiarotti, Matteo Cococcioni, Ismaila Dabo, Andrea Dal Corso, Stefano de Gironcoli, Stefano Fabris, Guido Fratesi, Ralph Gebauer, Uwe Gerstmann, Christos Gougoussis, Anton Kokalj, Michele Lazzeri, Layla Martin-Samos, Nicola Marzari, Francesco Mauri, Riccardo Mazzarello, Stefano Paolini, Alfredo Pasquarello, Lorenzo Paulatto, Carlo Sbraccia, Sandro Scandolo, Gabriele Sclauszero, Ari P Seitsonen, Alexander Smogunov, Paolo Umari, and Renata M Wentzcovitch. Quantum espresso: a modular and open-source software project for quantum simulations of materials. *Journal of Physics: Condensed Matter*, 21(39):395502 (19pp), 2009.
 - [28] Nicola Marzari, Arash A. Mostofi, Jonathan R. Yates, Ivo Souza, and David Vanderbilt. Maximally localized wannier functions: Theory and applications. *Rev. Mod. Phys.*, 84:1419–1475, Oct 2012.
 - [29] Arash A Mostofi, Jonathan R Yates, Young-Su Lee, Ivo Souza, David Vanderbilt, and Nicola Marzari. wannier90: A tool for obtaining maximally-localised wannier functions. *Computer physics communications*, 178(9):685–699, 2008.
 - [30] S Baumann, F Donati, S Stepanow, S Rusponi, W Paul, S Gangopadhyay, IG Rau, GE Pacchioni, L Gragnaniello, M Pivetta, et al. Origin of perpendicular magnetic anisotropy and large orbital moment in fe atoms on mgo. *Physical review letters*, 115(23):237202, 2015.
 - [31] JR Nicholls, DJ Hall, and PF Tortorelli. Hardness and modulus measurements on oxide scales. *Materials at high temperatures*, 12(2-3):141–150, 1994.
 - [32] Sign change in F_W is equivalent to a 45-degree rotation
 - [33] Small variations in D_W do not influence the low energy spectra